

MICROGRAVITY EXPERIMENT OF ROCK CLIMBING LOCOMOTION FOR EXPLORATION ROBOT ON MINOR BODY

*Yudai Yuguchi¹, Wudom Tesshin¹, Kyohei Maruya¹, Kenji Nagaoka¹ and Kazuya Yoshida¹

¹ *Tohoku University, Aoba 6-6-01, Aramaki, Aoba-ku, Sendai, Japan, E-mail: {yuguchi, u-domu, maruya, nagaoka, yoshida}@astro.mech.tohoku.ac.jp*

ABSTRACT

In this study, we analyze the motion of a type of rock-climbing robot used for minor body exploration. The surface of a minor body features an irregular terrain and microgravity. Hence, it is effective for an exploration robot to move by gripping the surface. In the robot's gait, the reaction force acting on the gripper of the supporting arm must be controlled to prevent the detachment of the gripper from the surface. Therefore, we formulate a control method to continue locomotion with reactionless motion by utilizing reaction null-space. Moreover, the control law is experimentally verified using an air floating system under microgravity. Furthermore, planar simulation shows that a reactionless axis affects continuous locomotion.

1 INTRODUCTION

With rapid advances in space development, the interest in minor body exploration has been constantly increasing. An example of pioneering a spacecraft for minor body exploration includes the NEAR-Shoemaker, which successfully landed on asteroid Eros and captured high-resolution photos of its surface [1]. The Japanese spacecraft Hayabusa2 was launched in 2014 and is expected to reach the asteroid Ryugu in 2018 [2]. Minor bodies are expected to possess evidences revealing the evolutionary process of our solar system. Thus, implementing minor body exploration is highly significant. In particular, unmanned exploration using robots is effective for detailed investigations of minor body surfaces. Such robots are required to have the ability to reach a scientifically significant area; however, it is difficult for them to move on such surfaces. This is because these surfaces are unknown irregular terrains with extremely low gravity. In such environments, it is difficult for a robot to maintain its position on the surface, and it can easily float because of surface contact forces. Therefore, wheeled and legged mechanisms aimed at planetary exploration are unsuited for minor

body exploration [3]. Matsuno et al. proposed the use of a legged robot to control the contact with an asteroid surface [4]. However, a locomotive strategy was not mentioned. To address this issues, Yoshimitsu et al. proposed a hopping mobility system in MINERVA that was carried by the Japanese spacecraft Hayabusa [5]. This mechanism facilitated effective movement about an asteroid surface, and was implemented in other hopping robots [6], [7]. However, it is difficult for these robots to reach their specific location because of their repetitive bouncing locomotion. Furthermore, a robot that moves by ciliary vibrations has been studied; however, it is unsuitable for rough terrains [8].

For locomotive problems, Yoshida et al. proposed a type of rock-climbing robot [9]. In this paper, we refer to this robot as a "ground-gripping robot." By gripping the surface of a minor body, the robot can prevent its flotation and implement secure exploration activities. The robot gait can be divided into three phases, as shown in Fig. 1. Phase 1 comprises the motion of surface gripping. Thus far, we formulated a gripping condition for the case in which the gripper and surface are symmetric, as in [10]. After this phase, the arm gripping the surface becomes the renewed supporting arm. Phase 2 consists of the motion of detachment from the surface, and Phase 3 comprises the movement of the idling arm. By repeating this gait, the robot can continuously move on the surface. In this paper, we focus on Phase 3, in which motion control is required considering the reaction force acting on the gripper of the supporting arm. When the idling arm is moved, all reaction forces act on the gripper of the supporting arm. If the reaction force exceeds the gripping force, it detaches from the surface, and the robot's locomotion ceases. As an example of reaction control for space robots, Nenchev et al. proposed reactionless control that utilizes the reaction null-space [11]. As another approach, Wu et al. proposed the path planning of a manipulator using a genetic algorithm [12]. However, this method is unsuitable for the precise control of the tip position because the method is designed in joint

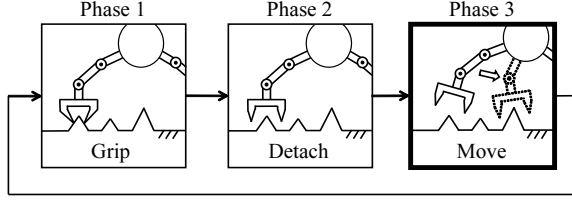


Figure 1: Locomotive gait of ground-gripping robot.

space. Furthermore, a calculated load for reactionless control is lesser than that for this method. We applied the reactionless control to the ground-gripping robot and clarified that the initial base height affects stable locomotion through planar simulation [13].

In this study, we verified reactionless locomotion in microgravity through an experiment and simulations. The equation of motion of the ground-gripping robot is first formulated, followed by the formulation of the simultaneous control law, combining the reactionless control and the control of the idling arm's tip position. Moreover, the effectiveness of the control method is confirmed through a single-step locomotion experiment using an air floating system. Finally, we show that the reactionless axis affects stable locomotion on irregular terrains through planar simulation and discuss singularities.

2 DYNAMICS OF GROUND-GRIPPING ROBOT

In this section, we first present a dynamic model of the ground-gripping robot, followed by its equation of motion.

2.1 Nomenclature

Fig. 2 shows the dynamic model of a dual-arm robot. The symbols used in this paper are defined below.

$\mathbf{F}_s \in \mathbb{R}^6$: Vector of force and momentum on the gripper of the supporting arm.

$\boldsymbol{\tau} \in \mathbb{R}^n$: Vector of torque on manipulator joints.

$\mathbf{H}_s \in \mathbb{R}^{6 \times 6}$: Inertial matrix of the gripper of the supporting arm.

$\mathbf{H}_m \in \mathbb{R}^{n \times n}$: Inertial matrix of the manipulator.

$\mathbf{H}_{sm} \in \mathbb{R}^{6 \times n}$: Inertial matrix of coupling between the gripper of the supporting arm and manipulator.

$\mathbf{x}_s \in \mathbb{R}^6$: Vector of the position and orientation of the gripper of the supporting arm.

$\boldsymbol{\phi} \in \mathbb{R}^n$: Vector of the joint angle of the manipulator.

$\mathbf{c}_s \in \mathbb{R}^6$: Nonlinear velocity-dependent term of the gripper of the supporting arm.

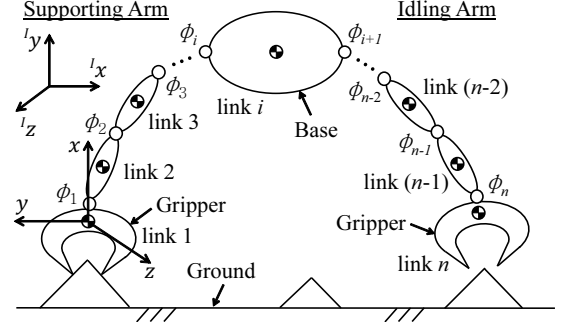


Figure 2: Dynamic model of ground-gripping robot.

$\mathbf{c}_m \in \mathbb{R}^n$: Nonlinear velocity-dependent term of the manipulator.

$\mathbf{J}_s \in \mathbb{R}^{6 \times 6}$: Jacobian matrix of the gripper of the supporting arm.

$\mathbf{J}_m \in \mathbb{R}^{6 \times n}$: Jacobian matrix of the manipulator.

$\mathbf{F}_h \in \mathbb{R}^6$: Vector of force and momentum on the manipulator's tip.

$\mathbf{H}^* \in \mathbb{R}^{n \times n}$: Generalized inertial matrix.

$\mathbf{c}^* \in \mathbb{R}^n$: Generalized nonlinear velocity-dependent term.

The “manipulator” represents links other than the gripper of the supporting arm.

2.2 Equation of Motion

For modeling the equation of motion, we made the following assumptions:

- The gravitational force is negligible.
- Contact forces do not act on the robot.
- At least one arm grips the surface.

By dividing all the links between the gripper of the supporting arm and the manipulator, the equation of motion is given as

$$\begin{bmatrix} \mathbf{F}_s \\ \boldsymbol{\tau} \end{bmatrix} = \begin{bmatrix} \mathbf{H}_s & \mathbf{H}_{sm} \\ \mathbf{H}_{sm}^T & \mathbf{H}_m \end{bmatrix} \begin{bmatrix} \ddot{\mathbf{x}}_s \\ \ddot{\boldsymbol{\phi}} \end{bmatrix} + \begin{bmatrix} \mathbf{c}_s \\ \mathbf{c}_m \end{bmatrix} - \begin{bmatrix} \mathbf{J}_s^T \\ \mathbf{J}_m^T \end{bmatrix} \mathbf{F}_h \quad (1)$$

The upper and lower parts of (1) denote the equations of motion about the gripper of the supporting arm and the manipulator, respectively. By assuming that contact forces do not act on the tip of the manipulator ($\mathbf{F}_h = \mathbf{0}$), and by eliminating the acceleration of the gripper of the supporting arm $\ddot{\mathbf{x}}_s$ from (1), the control torque $\boldsymbol{\tau}$ can be written as

$$\boldsymbol{\tau} = \mathbf{H}^* \ddot{\boldsymbol{\phi}} + \mathbf{c}^* + \mathbf{H}_{sm}^T \mathbf{H}_s^{-1} \mathbf{F}_s \quad (2)$$

where

$$\mathbf{H}^* \equiv \mathbf{H}_m - \mathbf{H}_{sm}^T \mathbf{H}_s^{-1} \mathbf{H}_{sm} \quad (3)$$

$$\mathbf{c}^* \equiv \mathbf{c}_m - \mathbf{H}_{sm}^T \mathbf{H}_s^{-1} \mathbf{c}_s \quad (4)$$

3 CONTROL LAW

In this section, we formulate the desired joint angular velocity. We first describe the reactionless constraint by utilizing the reaction null-space. Next, we present the simultaneous control law combining the tip position control and constraint using the task-priority method. Moreover, we explain the generation of the desired tip trajectory.

3.1 Reactionless Motion Control

We assume that no external force acts on the robot, and the initial linear and angular momenta with respect to the center of mass of the supporting arm's gripper are zero. In this case, the following conservation laws of linear momentum $\mathbf{P} \in \mathbb{R}^3$ and angular momentum $\mathbf{L}_0 \in \mathbb{R}^3$ can be established:

$$\begin{bmatrix} \mathbf{P} \\ \mathbf{L}_0 \end{bmatrix} = \mathbf{H}_s \dot{\mathbf{x}}_s + \mathbf{H}_{sm} \dot{\boldsymbol{\phi}} = \mathbf{0} \quad (5)$$

From (5), the condition whereby the momenta due to the gripper of the supporting arm are both zero is given as

$$\mathbf{H}_{sm} \dot{\boldsymbol{\phi}} = \mathbf{0} \quad (6)$$

As long as the manipulator moves under this constraint, the reaction force does not act on the gripper of the supporting arm. (6) represents the constraint on six dimensions with respect to the inertial frame. However, in this study, reactionless control is applied to a limited number of dimensions. Therefore, we formulated a revised condition by rewriting \mathbf{H}_{sm} as

$$\hat{\mathbf{H}}_{sm} \dot{\boldsymbol{\phi}} = \mathbf{0} \quad (7)$$

The desired joint angular velocity that satisfies (7) can be expressed as

$$\dot{\boldsymbol{\phi}}_d = \mathbf{R}_{RNS} \boldsymbol{\xi} \quad (8)$$

$$\mathbf{R}_{RNS} \equiv \mathbf{I} - \hat{\mathbf{H}}_{sm}^+ \hat{\mathbf{H}}_{sm} \quad (9)$$

where $\boldsymbol{\xi}$ and \mathbf{R}_{RNS} respectively denote an arbitrary vector and the projector on the null-space of the inertial coupling matrix $\hat{\mathbf{H}}_{sm}$. \mathbf{R}_{RNS} is called the reaction null-space.

Subsequently, the simultaneous control method combined with the tip position control is expressed through task-priority redundancy resolution. To enable the robot to continue locomotion, it is important that the gripper of the supporting arm does not detach from the surface. Therefore, we set reactionless motion control as the primary task.

The relationship between the manipulator's tip velocity $\dot{\mathbf{x}}_h$ and the joint angular velocity $\dot{\boldsymbol{\phi}}$ is generally expressed as

$$\dot{\mathbf{x}}_h = \mathbf{J}_m \dot{\boldsymbol{\phi}} \quad (10)$$

Substituting (8) into (10), vector $\boldsymbol{\xi}$ is calculated as

$$\boldsymbol{\xi} = \tilde{\mathbf{J}}_m^+ \mathbf{K} (\mathbf{x}_d - \mathbf{x}_h) \quad (11)$$

where $\tilde{\mathbf{J}}_m$ is expressed as

$$\tilde{\mathbf{J}}_m \equiv \mathbf{J}_m \mathbf{R}_{RNS} \quad (12)$$

In (11), $\dot{\mathbf{x}}_h$ is replaced by a control gain matrix \mathbf{K} and the desired tip position and orientation \mathbf{x}_d for the tip position control. Moreover, the superscript “+” represents the pseudo inverse. Furthermore, the desired joint angular velocity for simultaneous control is obtained by substituting (11) into (8) as

$$\dot{\boldsymbol{\phi}}_d = \mathbf{R}_{RNS} \tilde{\mathbf{J}}_m^+ \mathbf{K} (\mathbf{x}_d - \mathbf{x}_h) \quad (13)$$

3.2 Measurement of Manipulability

A reactionless motion control utilizing the reaction null-space comprises dynamic and algorithmic singularities [14]. Thus, we devised three types of equations for measuring each manipulability. The manipulability measures u and v regarding dynamic singularity are expressed as

$$u \equiv \sqrt{|\hat{\mathbf{H}}_{sm} \hat{\mathbf{H}}_{sm}^T|} \quad (14)$$

$$v \equiv \sqrt{|\mathbf{J}_m \mathbf{J}_m^T|} \quad (15)$$

Moreover, the manipulability measure w regarding algorithmic singularity is presented as

$$w \equiv \sqrt{|\mathbf{J}_q \mathbf{J}_q^T|} \quad (16)$$

where \mathbf{J}_q is expressed as

$$\mathbf{J}_q \equiv \tilde{\mathbf{J}}_m \mathbf{R}_{RNS}^+ \quad (17)$$

3.3 Tip Trajectory Generation

As the gripper of the idling arm moves away from and then close to the minor body's surface, unintended contact and friction between the gripper and surface must be avoided. When the contact or frictional force exceeds the gripping force of the supporting arm's gripper, the gripper detaches from the surface. Thus, the robot cannot maintain stable locomotion. In response to this demand, the trajectory whereby the gripper of the idling arm is vertically moved away from and then close to the surface is generated in two dimensions. To satisfy this condition, the trajectory is made elliptical so that the trajectory from the initial tip position in Phase 3 to its desired position is connected smoothly. Fig. 3 shows a model of the elliptical trajectory, in which \mathbf{x}_0 denotes the vector of

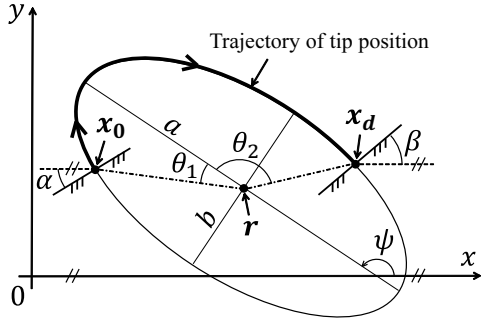


Figure 3: Model of elliptical trajectory.

the initial tip position. The coordinates of the initial and desired tip positions can be written as

$$x_{0x} = a \cos \theta_1 \cos \psi - b \sin \theta_1 \sin \psi + r_x \quad (18)$$

$$x_{0y} = a \cos \theta_1 \sin \psi + b \sin \theta_1 \cos \psi + r_y \quad (19)$$

$$x_{dx} = a \cos \theta_2 \cos \psi - b \sin \theta_2 \sin \psi + r_x \quad (20)$$

$$x_{dy} = a \cos \theta_2 \sin \psi + b \sin \theta_2 \cos \psi + r_y \quad (21)$$

where a , b , θ , ψ , and $\mathbf{r} (= [r_x, r_y]^T)$ denote the length of the long axis of an ellipse, the length of its short axis, the angle between the long axis and tip position, the inclination angle of the ellipse, and the vector of the central coordinates of the ellipse, respectively. Furthermore, conditional equations whereby the tip of the idling arm moves away from and then close to the surface in a direction perpendicular to it are expressed as

$$\left| a \tan \left(\frac{dy}{dx} \Big|_{\theta=\theta_1} \right) - \alpha \right| \leq \epsilon_0 \quad (22)$$

$$\left| a \tan \left(\frac{dy}{dx} \Big|_{\theta=\theta_2} \right) - \beta \right| \leq \epsilon_d \quad (23)$$

where α and β denote the tangent angles of the ellipse at the initial and desired tip positions, respectively. Moreover, the acceptable error ranges ϵ_0 and ϵ_d are set to address cases in which a perfect elliptical trajectory cannot be generated vertical to the surface. By solving the constrained non-linear optimization problem using (18) - (23), the desired elliptical trajectory is generated.

4 LOCOMOTION EXPERIMENT

In this section, we describe our experiment of single-step locomotion according to the control law stated in Section 3. In this experiment, we used an air floating system to emulate motion in microgravity. We first present the configuration of the air floating system, followed by the experimental conditions. Next, we verify gait control by comparing motion with and without the reactionless control law.

4.1 Air Floating System

To validate the gait control method, we developed an air floating system, as shown in Fig. 4. Table 1 lists the link parameters. Link 1 denotes the gripper of the supporting arm, and the gripping state was simulated by setting the inertial parameters to large virtual values. The gripper of the supporting arm was fixed on a flat plate mounted on the side of the surface plate. This system can float on the surface of the plate by emitting compressed air stored in an air tank by using air bearings mounted at the bottom of the system. There was almost no friction between the system and surface plate, and the system simulated the motion in planar microgravity. Furthermore, this system had four degrees-of-freedom (DOF) and used motors (RH-8D-3006-E100AL) manufactured by Harmonic Drive Systems Inc. Each tip was equipped with a force/torque sensor (WDF-6M200-3) produced by WACOH-TECH Inc.

4.2 Experimental Conditions

In this experiment, the reactionless axis was set parallel to the minor body's surface gripped by the gripper of the supporting arm. This is to prevent the sideslip of the rock being gripped due to the motion of the idling arm. Moreover, the initial angles of each joint were set as $\phi = [35^\circ, -35^\circ, -35^\circ, 35^\circ]$. The desired tip position of the idling arm was set at +0.08 m along the ${}^I x$ -axis and +0.04 m along the ${}^I y$ -axis from the initial tip position, and the desired tip posture was set at -60° , relative to the ${}^I x$ -axis. The tip posture angle was controlled at a constant rate during movement. These desired values simulated the motion of the robot climbing up a slope. Further, the control time, measurement time, and control gain were set at 16 s, 18 s, and $\mathbf{K} = \text{diag}(2, 2, 2)$ in both cases.

4.3 Experimental Results

Fig. 5 shows the motion sequences of the air floating system when reactionless control is incorporated. Fig. 6 shows the reaction forces with and without reactionless control. Fig. 6 (a) shows that approximately 0.5 N of F_y was exerted on the tip of the supporting arm. Moreover, both forces in Fig. 6 (a) show that the robot moved while continuously vibrating because of joint stiffness. In contrast, Fig. 6 (b) shows that F_y remains close to zero and the vibration of the robot was suppressed. Thus, reactionless control law reduces the risk of sideslipping of the rock being gripped by the supporting arm's gripper and suppresses the vibration of the robot during motion. Moreover, Fig. 7 shows the tip position and posture of the system with the incorporation of reactionless control. Fig. 7 (a) shows that the control value is con-

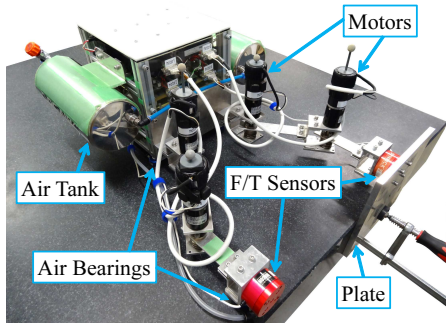


Figure 4: Air floating system.

sistent with the desired value, and the elliptical trajectory is realized. Furthermore, the tip posture angle γ in Fig. 7 (b) followed the desired value. Therefore, the validity of the gait control method was confirmed.

5 MOBILITY ANALYSIS

In this section, we apply two types of reactionless axes to the gait control law and verify the continuous locomotion of a ground-gripping robot on a rough terrain through planar simulation. We first present the simulation conditions, including the simulation model of the robot and the generation method of the rough terrain. In the simulation, the adaptability of each gait to the rough terrain is discussed in terms of the manipulability measure.

5.1 Simulation Conditions

In the simulation, a dual-arm robot with each arm having three DOF was used to improve manipulability over the air floating system. Table 2 lists the link parameters. Locomotion was simulated by switching the state quantities of the links corresponding to each arm when the tip of the idling arm reached the desired tip position and posture angle. Moreover, the simulation was executed by setting two reactionless axes. One was set parallel to the surface (case 1), and other was set vertical to the surface (case 2). In addition, case 2 is useful for preventing detachment of the gripper from the surface because the allowable reaction force in this direction depends on the gripping force. Furthermore, the reaction force acting on the gripper of the supporting arm \mathbf{F}_s was calculated

Table 1: Link parameters of air floating system

	mass [kg]	inertia [kg·m ²]	length [m]
link 1	1000	1×10^9	0.13597
link 2	0.565	0.00216655	0.14997
Base	9.690	0.15481713	0.15800
link 4	0.565	0.00216655	0.14997
link 5	0.350	0.00085437	0.13597

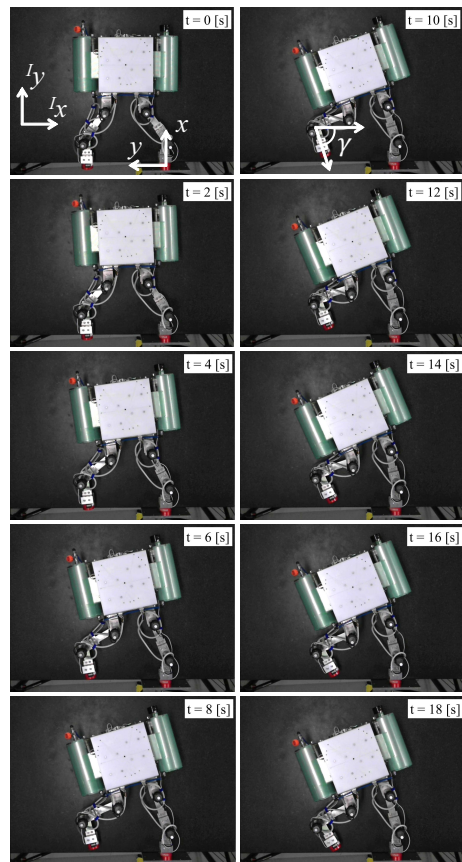


Figure 5: Motion sequence of air floating system.

by applying the following equation:

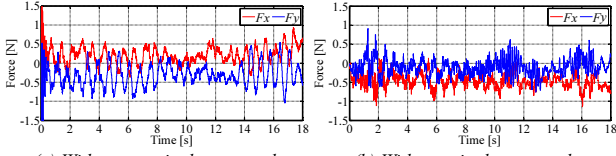
$$\mathbf{F}_s = -k_p \Delta \mathbf{x}_s - k_c \dot{\mathbf{x}}_s \quad (24)$$

where the parameters of stiffness k_p and viscosity k_c were set at 3000.

A minor body surface was simulated by randomly setting inclinations and heights of lines 9 mm apart along the X-axis, and connecting them with lines 1 mm apart along the X-axis. The range of the inclination was randomly set from -30° to $\sim 30^\circ$, relative to the X-axis. On the contrary, the range of the height was randomly set from -10 mm to ~ 10 mm according to the height of the previous line's center. Moreover, the initial angles of each joint were set at $\phi = [-15^\circ, -105^\circ, 30^\circ, 30^\circ, -105^\circ, -15^\circ]$. Further, the stride length along the X-axis, the control time in a single step, the number of motion cycles, the control gain, and the number of times the simulation was run were set at 0.04 m, 8 s, 8 cycles, $\mathbf{K} = \text{diag}(12, 12, 12)$, and 50 times, respectively.

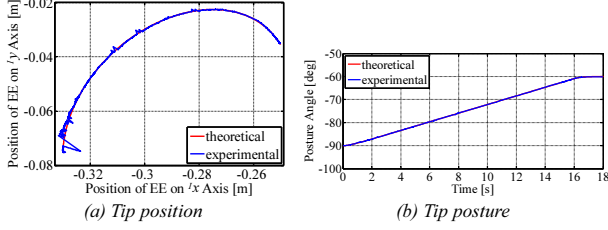
5.2 Simulation Results

Fig. 8 illustrates the motion sequences of the robot for case 1. Fig. 9 and Fig. 10 show the reaction forces acting on the gripper of the supporting arm and the



(a) Without reactionless control (b) With reactionless control

Figure 6: Reaction forces acting on the tip of the supporting arm.



(a) Tip position (b) Tip posture

Figure 7: Tip position and posture of the idling arm.

manipulability measures, respectively. Fig. 9 depicts that almost no reaction force acted in the direction parallel to the surface. However, Fig. 10 (b) shows that the calculation entered algorithmic singularity while the robot was moving. The calculations for not only this surface type but also for all surface types were diverged in case 1. This is because the base moves in the opposite direction of locomotion to accomplish the reactionless gait.

On the contrary, Fig. 11 illustrates the motion sequences of case 2. Fig. 12 and Fig. 13 show the reaction forces acting on the gripper of the supporting arm and the manipulability measures, respectively. In case 2, there are many situations in which the robot was able to move across the surface for all motion cycles, and the number of divergences was 8. The divergences were caused by ingress to the algorithmic singularity such as in case 1. Therefore, it is clarified that the reactionless axis affects the stable locomotion of a ground-gripping robot. Furthermore, it is necessary to construct a control law for avoiding or passing through algorithmic singularity.

Table 2: Link parameters of simulation robot

	mass [kg]	inertia [kg·m ²]	length [m]
link 1	1000	1×10^9	0.050
link 2	0.30	0.0001675	0.080
link 3	0.30	0.0001675	0.080
Base	2.0	0.003333	0.10
link 5	0.30	0.0001675	0.080
link 6	0.30	0.0001675	0.080
link 7	0.50	0.0001167	0.050

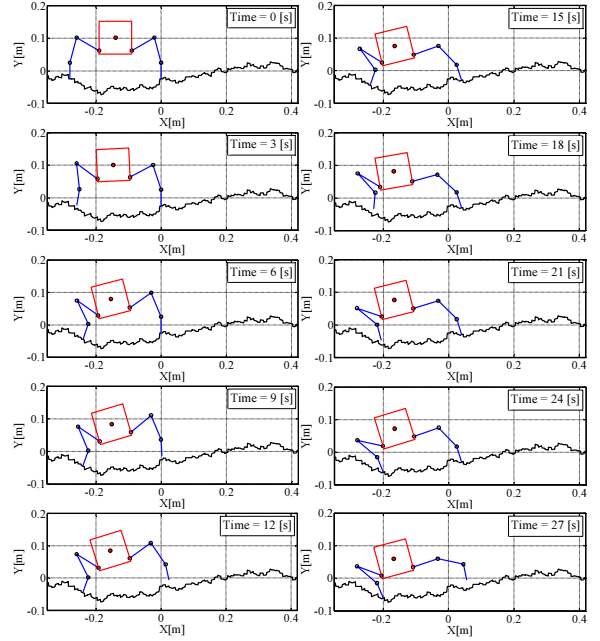
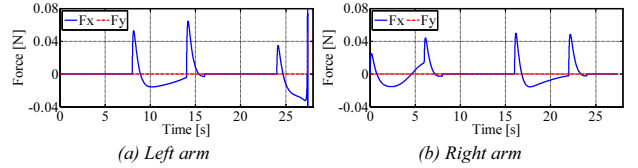
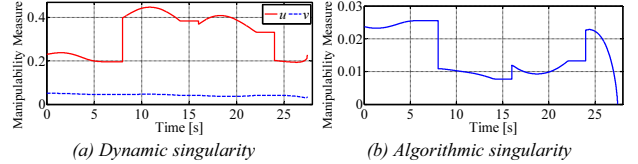


Figure 8: Robot motion sequence in case 1.



(a) Left arm (b) Right arm

Figure 9: Reaction forces in case 1.



(a) Dynamic singularity (b) Algorithmic singularity

Figure 10: Manipulability measures in case 1.

6 CONCLUSIONS

In this paper, we focused on the reaction forces acting on the tip of the supporting arm of a ground-gripping robot, and proposed a reactionless gait for stable locomotion. Moreover, we verified the effectiveness through an experiment and simulations. We first described the equation of motion of the ground-gripping robot, followed by the simultaneous control law using the reaction null-space. In addition, the manipulability measures and generation of the elliptical tip trajectory were formulated. Furthermore, we developed an air floating system, and confirmed a single-step locomotion through the experiment. We then conducted two types of simulations of continuous locomotion on irregular terrain. The result showed the reactionless axis affects the feasibility of the robot.

In future research, we plan to develop a gripper suitable for the environment of a minor body and ver-

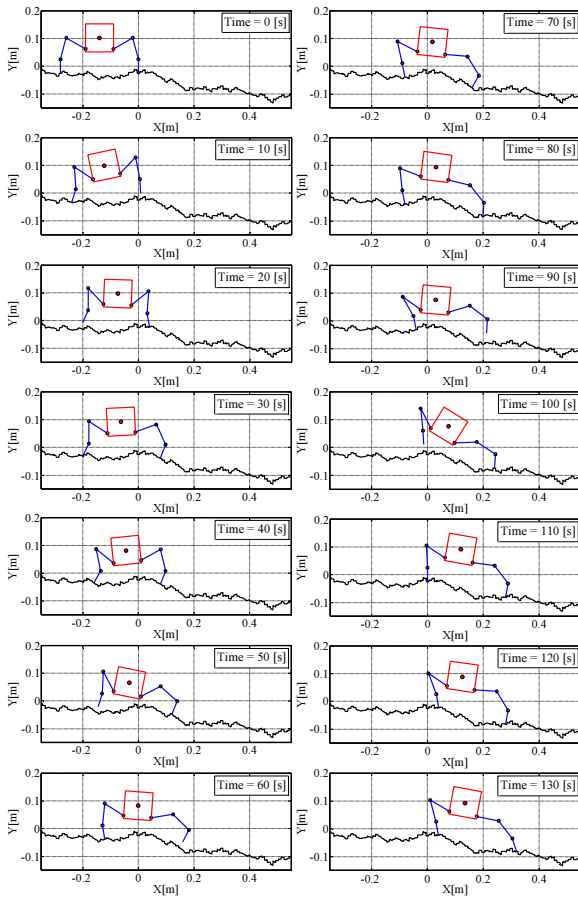
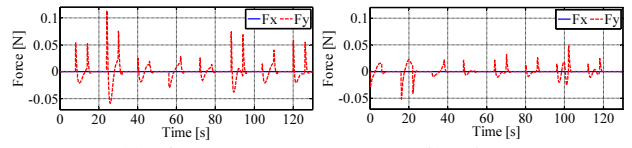


Figure 11: Robot motion sequence in case 2.

ify the continuous locomotion using our air floating system. Moreover, we need to address algorithmic singularity to accomplish stable locomotion on any irregular terrain.

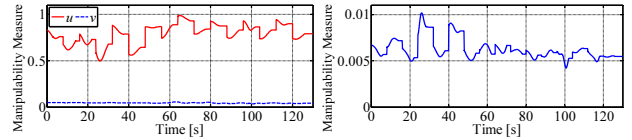
References

- [1] J. Veverka, et al. "The Landing of the NEAR-Shoemaker Spacecraft on Asteroid 433 Eros," *Nature*, vol. 413, issue 6854, pp. 390-393, 2001.
- [2] Y. Tsuda, et al. "Flight Status of Robotic Asteroid Sample Return Mission Hayabusa2," *Acta Astronautica*, 2016. (in press) (doi: 10.1016/j.actaastro.2016.01.027)
- [3] S. Nishikori, S. Hokamoto and T. Kubota, "Kinematic Discussion and Development of a Multi-Legged Planetary Exploration Rover with an Isotropic Leg Arrangement," *Advanced Robotics*, vol. 25, Issue 6-7, pp. 789-804, 2011.
- [4] F. Matsuno and Y. Oosako, "Experimental Study on Control of an Asteroid Sample Return Robot during Contact based on Complementarity Modeling," *Proc. 2002 IEEE International Conference on Robotics and Automation*, pp. 2283-2288, 2002.
- [5] T. Yoshimitsu, et al. "Micro-Hopping Robot for Asteroid Exploration," *Acta Astronautica*, vol. 52, pp. 441-446, 2003.



(a) Left arm (b) Right arm

Figure 12: Reaction forces in case 2.



(a) Dynamic singularity (b) Algorithmic singularity

Figure 13: Manipulability measures in case 2.

- [6] J. Burdick and P. Fiorini, "Minimalist Jumping Robots for Celestial Exploration," *The International Journal of Robotics Research*, vol. 22, no. 7-8, pp. 653-674, 2003.
- [7] Y. Nakamura, S. Shimoda and S. Shoji, "Mobility of a Microgravity rover using Internal Electro-Magnetic Levitation," *Proc. 2000 IEEE/RSJ International Conference on Intelligent Robots and Systems*, pp. 1639-1645, 2000.
- [8] K. Nagaoka and K. Yoshida, "Modeling and Analysis of Ciliary Micro-Hopping Locomotion Actuated by an Eccentric Motor in a Microgravity," *Proc. 2013 IEEE/RSJ International Conference on Intelligent Robots and Systems*, pp. 763-768, 2013.
- [9] K. Yoshida, T. Maruki and H. Yano, "A Novel Strategy for Asteroid Exploration with a Surface Robot," *Proc. 34th COSPAR Scientific Assembly*, pp. 281-286, 2002.
- [10] Y. Yuguchi, et al. "Experimental Evaluation of Gripping Characteristics Based on Frictional Theory for Ground Grip Locomotive Robot on an Asteroid," *Proc. 2015 IEEE International Conference on Robotics and Automation*, pp. 2822-2827, 2015.
- [11] D. N. Nenchev, et al. "Reaction Null-Space Control of Flexible Structure Mounted Manipulator Systems," *IEEE Transactions on Robotics and Automation*, vol. 15, no. 6, pp. 1011-1023, 1999.
- [12] J. Wu, et al. "Path Planning for Minimizing Base Reaction of Space Robot and its Ground Experimental Study," *Proc. 2009 IEEE International Conference on Mechatronics and Automation*, pp. 4627-4632.
- [13] Y. Yuguchi, et al. "Analysis on Motion Control Based on Reaction Null Space for Ground Grip Robot on an Asteroid," *Proc. 30th International Symposium on Space Technology and Science*, 2015-k-73, 2015.
- [14] M. Jin, et al. "Cartesian Path Planning for Base Attitude Adjustment of Space Robot," *Proc. 2015 IEEE International Conference on Mechatronics and Automation*, pp. 582-587.